Synthesis and Bonding in the Diamagnetic Dinuclear Tantalum(IV) Hydride Species $([P_2N_2]Ta)_2(\mu\text{-}H)_4$ and the Paramagnetic Cationic Dinuclear Hydride Species $\{([P_2N_2]Ta)_2(\mu\text{-}H)_4\}^+I^-$ ($[P_2N_2]$ = $PhP(CH_2SiMe_2NSiMe_2CH_2)_2PPh$): The Reducing Ability of a Metal−Metal Bond

Michael D. Fryzuk,* Samuel A. Johnson, and Steven J. Rettig†

Department of Chemistry, University of British Columbia, 2036 Main Mall, Vancouver, British Columbia, Canada V6T 1Z1

Received April 26, 2000

The controlled reaction of the Ta(V) trimethyl species $[P_2N_2]TaMe_3$, where $[P_2N_2]$ = $PhP(CH_2SiMe_2NSiMe_2CH_2)_2PPh$, under 0.5 atm of hydrogen gas produces a partially hydrogenated Ta(V) species, $([P_2N_2]TaMe_2(H)$, of unknown structure. Under 4 atm of hydrogen gas, further hydrogenation does not produce the complex $[P_2N_2]TaH_3$; instead, reduction of the tantalum center occurs to yield the dinuclear Ta(IV) hydride $([P_2N_2]Ta)_2(\mu\text{-}H)_4$. This diamagnetic tetrahydride fails to react with many reagents, including ethylene and carbon monoxide; however, upon addition of iodomethane, $\{([P_2N_2]Ta)_2(\mu\text{-}H)_4\}^+I^-$ is produced as a paramagnetic green crystalline solid. The number of hydrides in this reaction product was confirmed by a deuterium labeling study. The results of a variable-temperature magnetic susceptibility study of this tetrahydride cation can be partially modeled with the Curie−Weiss law and a large correction for temperature-independent magnetism. Ab initio calculations using density functional theory were performed in an attempt to further understand the influence of the macrocyclic ligand in the bonding in these complexes.

Introduction

There have been several reports of metal−metal bonds storing electrons that were later utilized in the reduction of dinitrogen. For example, we have reported that the hydrogenation of the Ta(V) complex $[NPN]TaMe_3$, where [NPN] = $PhP(CH_2SiMe_2NPh)_2$, generates the dinuclear Ta(IV) tetrahydride $([NPN]Ta)_2(\mu\text{-}H)_4$; because this complex is diamagnetic, it can be described as containing a tantalum−tantalum single bond. What is particularly significant about this dinuclear complex is that it reacts with dinitrogen with the elimination of 1 equiv of hydrogen gas to generate $([NPN]Ta)_2(\mu\text{-}H)_2(\mu\text{-}\eta^1\text{:}\eta^2\text{-}N_2)$. This formally corresponds to an overall four-electron reduction of dinitrogen, where two electrons were initially stored in a metal−metal bond.[1] The reduction of dinitrogen by electrons stored in a metal−metal single bond has also recently been described for a niobium dinitrogen complex,[2,3] and metal−metal bonding interactions have also been implicated in storing electrons for the reduction of dinitrogen in nitrogenase.[4]

Herein, we describe the use of the $[P_2N_2]$ ligand (where $[P_2N_2]$ = $PhP(CH_2SiMe_2NSiMe_2CH_2)_2PPh$) to generate the complex $([P_2N_2]Ta)_2(\mu\text{-}H)_4$, which is diamagnetic and contains a tantalum−tantalum bond. Unlike the complex $([NPN]Ta)_2(\mu\text{-}H)_4$, the more coordinatively saturated complex $([P_2N_2]Ta)_2(\mu\text{-}H)_4$ does not react with dinitrogen; however, attempts to remove the hydride ligands utilizing electrophiles demonstrates that the primary reactivity of this complex is as a reducing agent.

Results and Discussion

We have previously reported the preparation of $[P_2N_2]TaMe_3$ and its photochemical conversion to the Ta(V) methylidene complex $[P_2N_2]Ta{=}CH_2(Me)$.[5] The macrocyclic ancillary ligand $[P_2N_2]$[6] is a flexible framework of two amido and two phosphine donors that have been shown to stabilize complexes of the early transition metals,[7−9] the main-group elements,[10] and the lan-

† Professional Officer: UBC X-ray Structural Laboratory (deceased October 27, 1998).

(1) Fryzuk, M. D.; Johnson, S. A.; Rettig, S. J. *J. Am. Chem. Soc.* **1998**, *120*, 11024−11025.
(2) Caselli, A.; Solari, E.; Scopelliti, R.; Floriani, C.; Re, N.; Rizzoli, C.; Chiesi-Villa, A. *J. Am. Chem. Soc.* **2000**, *122*, 3652−3670.
(3) Zanoti-Gerosa, A.; Solari, E.; Giannini, L.; Floriani, C.; Chiesi-Villa, A.; Rizzoli, C. *J. Am. Chem. Soc.* **1998**, *120*, 437.
(4) Han, J.; Beck, K.; Ockwig, N.; Coucouvanis, D. *J. Am. Chem. Soc.* **1999**, *121*, 10448.
(5) Fryzuk, M. D.; Johnson, S. A.; Rettig, S. J. *Organometallics* **1999**, *18*, 4059−4067.
(6) Fryzuk, M. D.; Love, J. B.; Rettig, S. J. *J. Chem. Soc., Chem. Commun.* **1996**, 2783.
(7) Basch, H.; Musaev, D. G.; Morokuma, K.; Fryzuk, M. D.; Love, J. B.; Seidel, W. W.; Albinati, A.; Koetzle, T. F.; Klooster, W. T.; Mason, S. A.; Eckert, J. *J. Am. Chem. Soc.* **1999**, *121*, 523−528.
(8) Fryzuk, M. D.; Love, J. B.; Rettig, S. J.; Young, V. G. *Science* **1997**, *275*, 1445.
(9) Fryzuk, M. D.; Love, J. B.; Rettig, S. J. *Organometallics* **1998**, *17*, 846−853.
(10) Fryzuk, M. D.; Giesbrecht, G. R.; Rettig, S. J. *Inorg. Chem.* **1998**, *37*, 6928−6934.

10.1021/om000359w CCC: $19.00
Publication on Web 08/24/2000

thanides[11] in a variety of geometries. The ready availability of the trimethyl complex $[P_2N_2]TaMe_3$ prompted us to further examine its reactivity patterns.

Hydrogenation of $[P_2N_2]TaMe_3$ and Structure of $([P_2N_2]Ta)_2(\mu\text{-}H)_4$ (1). A solution of $[P_2N_2]TaMe_3$ under 4 atm of dihydrogen gradually darkens from light yellow to a dark brick red. As monitored by $^{31}P\{^1H\}$ NMR spectroscopy, this reaction takes 3 days to go to completion. Examining the gases produced by GC-MS demonstrated that methane was the only product of this reaction; no ethane was observed. When this reaction is performed in hexanes, the product precipitates as a dark red-brown crystalline solid. The dark color of the product (λ_{max} 455 nm, $\epsilon = 6200$) is not consistent with a Ta(V) species; likewise, the ^1H NMR spectrum is not consistent with the anticipated Ta(V) hydrogenation product $[P_2N_2]TaH_3$. The only non-$[P_2N_2]$ ligand resonance in the ^1H NMR spectrum occurs at δ 5.86. This signal accounts for two hydride ligands per metal center and is a quintet due to coupling to four equivalent phosphorus-31 nuclei. From these data, the hydrogenation product can be assigned as the dimeric Ta(IV) hydride $([P_2N_2]Ta)_2(\mu\text{-}H)_4$ (**1**) as illustrated in eq 1. The diamagnetism of hydride **1** can be explained by the formation of a tantalum−tantalum σ-bond.

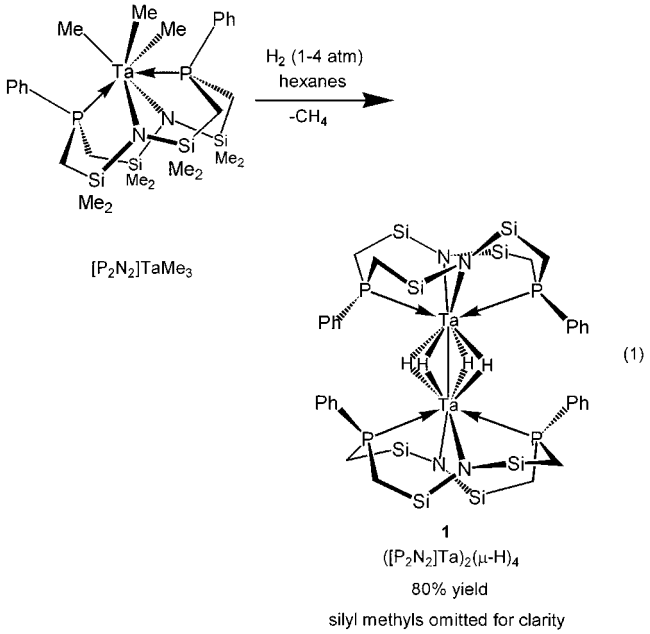

(1)

The solid-state molecular structure as determined by X-ray crystallography is shown in Figure 1. Crystallographic data are given in Table 1. Although there is no crystallographically imposed symmetry to the molecule in the solid-state structure, the molecule has approximate D_2 symmetry, with a C_2 axis running through the Ta−Ta bond and two perpendicular C_2 axes that are oriented through the center of the Ta(1)−Ta(2) bond that pass between, rather than through, the tantalum hydrides.

Additional symmetry elements are lacking, due to a twist in the $[P_2N_2]$ ligand backbone such that the Ta(2)−Ta(1)−N(1)−Si(1) torsion angle is 129.6(4)°, rather than near 90°. This twist has been noted before in other

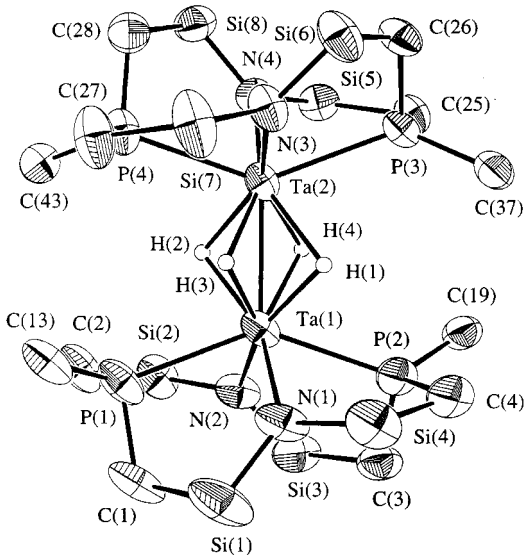

Figure 1. ORTEP diagram of the solid-state molecular structure of $([P_2N_2]Ta)_2(\mu\text{-}H)_4$ (**1**), as determined by X-ray crystallography. Silyl methyls have been omitted for clarity, and only the ipso carbons of the phenyl rings attached to phosphorus are shown. Selected bond distances (Å), bond angles (deg), and torsion angles (deg): Ta(1)−Ta(2), 2.6165(5); Ta−P(average) 2.615(3); Ta−N(average), 2.217(6); Ta(1)−H(1), 1.80(6); Ta(1)−H(2), 1.87(6); Ta(1)−H(3), 1.853(11); Ta(1)−H(4), 1.856(11); Ta(2)−H(1), 1.91(6); Ta(2)−H(2), 1.93(6); Ta(2)−H(3), 1.847(11); Ta(2)−H(4), 1.851(11); P(1)−Ta(1)−P(2), 139.87(9); Ta(2)−Ta(1)−P(1), 110.02(7); N(1)−Ta(1)−N(2), 101.7(2); Ta(2)−Ta(1)−N(1), 129.3(2); P(1)−Ta(1)−Ta(2)−P(4), −3.00(9); N(1)−Ta(1)−Ta(2)−N(4), 10.0(3); Ta(2)−Ta(1)−N(1)−Si(1), 129.6(4).

structurally characterized $[P_2N_2]$ complexes;[5] however, unlike in other cases, the twist in this case does not appear to be fluxional in solution. The room-temperature ^1H NMR spectrum contains four silyl methyl environments. If the twist in the ligand backbone were not rigid, only two silyl methyl signals would be anticipated, corresponding to silyl methyl groups directed toward the front and the back of the $[P_2N_2]$ ligand on each $[P_2N_2]$ unit.

While this locked conformation of the $[P_2N_2]$ ligand may arise from electronic effects due to the interaction of the amide lone pairs with tantalum metal orbitals, it may also be explained by steric interactions between the $[P_2N_2]$ ligands imposed by other electronic factors. The opposing $[P_2N_2]$ ligands on Ta(1) and Ta(2) are eclipsed, with a negligible P(1)−Ta(1)−Ta(2)−P(4) torsion angle of −3.00(9)°. This eclipsed arrangement of the $[P_2N_2]Ta$ units is likely of electronic origin, as sterically it appears less favorable; in this orientation the phenyl rings attached to phosphorus point away from each other only because of the twist in the $[P_2N_2]$ framework. For this twist in the conformation of the $[P_2N_2]$ framework to be fluxional, the $[P_2N_2]Ta$ units would have to be able to rotate with respect to each other, as steric interactions between phenyl groups on opposing $[P_2N_2]$ ligands prevent this twisting motion with the $[P_2N_2]$ ligands eclipsed. The solution ^1H NMR spectrum therefore confirms that the solution structure is identical with the solid-state structure and that the $[P_2N_2]$ conformation and orientation with respect to the opposing $[P_2N_2]$ ligand is rigid in solution.

(11) Fryzuk, M. D.; Love, J. B.; Rettig, S. J. *J. Am. Chem. Soc.* **1997**, *119*, 9071−9072.

Table 1. Crystal Data and Structure Refinement for 1 and 3

	1[a]	**3**[b]
formula	$C_{48}H_{88}N_4P_4Si_8Ta_2$	$C_{48}H_{88}IN_4P_4Si_8Ta_2$
fw	1431.72	1558.63
color, habit	red, prism	green needle
cryst size, mm	0.15 × 0.20 ×0.25	0.50 × 0.35 × 0.15
cryst syst	monoclinic	trigonal
space group	$P2_1/n$ (No. 14)	$P3_12_1$ (No. 152)
a, Å	12.748(3)	19.2489(7)
b, Å	21.186(2)	
c, Å	23.919(2)	14.9628(2)
α, deg	90	90
β, deg	101.857(11)	90
γ, deg	90	120
V, Å^3	6321.8(17)	4801.3(2)
Z	4	3
T, °C	21.0	−93
ρ_{calcd}, g/cm^3	1.504	1.616
F(000)	2888.00	2322.00
radiation	Mo	Mo
μ, cm^{-1}	31.41	41.77
transmissn factors	0.498−1.000	0.7594−1.0000
scan type	$\omega-2\theta$	ω
scan range in ω, deg	1.10 + 0.35 tan θ	
scan speed, deg/min	16 (up to 9 rescans)	
$2\theta_{max}$, deg	55	60.1
cryst decay, %	1.19	negligible
total no. of rflns	15 507	42 796
no. of unique rflns	14 853	4600
R_{merge}	0.061	0.072
no. of rflns with $I \geq n\sigma(I)$	5751	4481
no. of variables	610	303
R	0.037[a]	0.079[b]
R_w	0.029[a]	0.058[b]
GOF	1.65	1.19
max Δ/σ	0.003	0.03
residual density e/Å^3	0.77, −0.85 (both near Ta)	4.41 (near Ta), −3.25

[a] Rigaku AFC6S diffractometer: $R = \sum||F_o| - |F_c||/\sum|F_o|$; $R_w = (\sum w(|F_o| - |F_c|)^2/\sum w|F_o|^2)^{1/2}$. [b] Rigaku/ADSC CCD diffractometer: $R = \sum||F_o^2| - |F_c^2||/\sum|F_o^2|$; $R_w = (\sum w(|F_o^2| - |F_c^2|)^2/\sum w|F_o|^4)^{1/2}$.

As expected, the $[P_2N_2]$ ligand has an influence on the geometry at each tantalum center. The amide nitrogens are approximately *cis*-disposed, with a N(1)−Ta(1)−N(2) angle of 101.7(2)°. The phosphine donors are closer to a *trans* disposition, with a P(1)−Ta(1)−P(2) angle of 139.87°.

The Ta−Ta distance of 2.6165(5) Å is within that expected for a metal−metal bonding interaction but longer than in structurally related tantalum complexes; shorter Ta−Ta distances of 2.511(2) and 2.5359(4) Å were reported for the complexes $[Cl_2(PMe_3)_2Ta]_2(\mu\text{-}H)_4$[12] and $[(cb)(PMe_2Ph)_2(H)Ta]_2(\mu\text{-}H)_4$,[13] where cbH is 9H-carbazole. Longer Ta−Ta interactions of 2.854(1) and 2.8280(4) Å have also been observed in the compounds $(C_5Me_4Et)_2ClTa(\mu\text{-}H)_2TaCl_2(C_5Me_4Et)$[14] and $[(CyN)_2ClTa]_2(\mu\text{-}H)_2$,[15,16] where the tantalum centers are bridged by only two hydrides, as well as in the compound $[(Bu^t{}_3SiO)_2(H)_2Ta]_2$,[17] where an unbridged Ta−Ta distance of 2.720(4) Å was reported. The long Ta−Ta distance in **1** compared to those in the closely related $[Cl_2(PMe_3)_2Ta]_2(\mu\text{-}H)_4$[12] and $[(cb)(PMe_2Ph)_2(H)Ta]_2(\mu\text{-}H)_4$[13] may be due to the steric repulsion between the ligands on the metal centers, or perhaps due to the competition of the π-electrons of the amido donors for metal orbitals utilized in bridging the metal−metal bond, as will be discussed later in the section on bonding considerations.

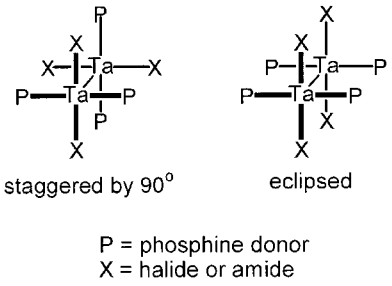

Figure 2. Depiction of "staggered by 90°" and "eclipsed" ligand arrangements.

The metal hydride atoms in hydride **1** were identified in electron density difference maps, and their locations were refined, though with distance constraints for H(3) and H(4). The bridging hydrides are staggered 45° with respect to the ligand donors, so that the hydride atoms lie between the planes described by P(1)−Ta(1)−P(2) and N(1)−Ta(1)−N(2). Not considering the Ta−Ta bond, the geometry at each tantalum center is approximately square-antiprismatic. The tantalum hydride distances determined from the X-ray data range from 1.80(6) Å to 1.93(6) Å, similar to those in $[Cl_2(PMe_3)_2Ta]_2(\mu\text{-}H)_4$, where the Ta−H bond length is 1.81(21) Å as determined from X-ray crystallography,[12] and the related rhenium complex $Re_2H_8(PEtPh)_4$, where the Re−H distance is 1.878(7) Å as determined from neutron diffraction data.[18]

Not surprisingly, the structure of species **1** is similar to that of the aforementioned compound $[Cl_2(PMe_3)_2Ta]_2(\mu\text{-}H)_4$;[12] however, the structural differences are intriguing. While the end groups in $[Cl_2(PMe_3)_2Ta]_2(\mu\text{-}H)_4$ are eclipsed, as in **1**, the phosphine ligands on opposing tantalum centers are staggered by 90°. Eclipsed and staggered by 90° could have various meanings in the context of these complexes; it is intended here to describe the eclipsed and staggered by 90° geometries that are depicted in Figure 2. Similar staggered by 90° ligand arrangements have been observed in the group 6 quadruple metal−metal bonded dimers $Mo_2Cl_4(PMe_3)_4$ and $W_2Cl_4(PMe_3)_4$,[19] although examples of the eclipsed ligand conformation are known both in metal−metal bonded complexes as well as in a dinuclear tantalum hydride featuring the 9H-carbazole amido ligand, $[(cb)(PMe_2Ph)_2(H)Ta]_2(\mu\text{-}H)_4$.[13] The $[P_2N_2]$ ligand clearly has an influence on the bonding in **1**, either via electronic effects caused by the difference in the bonding of the amides vs chlorides, slightly modified phosphines, or the geometrical restrictions of the macrocyclic ligand or via the steric interactions of the $[P_2N_2]$ ligand. The theoretical aspects of the bonding in **1** will be addressed in

(12) Scioly, A. J.; Luetkens, M. L. J.; Wilson, R. B.; Huffman, J. C.; Sattelberger, A. P. *Polyhedron* **1987**, *6*, 741−757.
(13) Profilet, R. D.; Fanwick, P. E.; Rothwell, I. P. *Polyhedron* **1992**, *11*, 1559−1561.
(14) Belmonte, P. A.; Schrock, R. R.; Day, C. S. *J. Am. Chem. Soc.* **1982**, *104*, 3082−3089.
(15) Cotton, F. A.; Daniels, L. M.; Murillo, C. A.; Wang, X. *J. Am. Chem. Soc.* **1996**, *118*, 12449−12450.
(16) Scoles, L.; Ruppa, K. B. P.; Gambarotta, S. *J. Am. Chem. Soc.* **1996**, *118*, 2529−2530.
(17) Miller, R. L.; Toreki, R.; LaPointe, R. E.; Wolczanski, P. T.; Van Duyne, G. D.; Roe, D. C. *J. Am. Chem. Soc.* **1993**, *115*, 5570−5588.
(18) Bau, R.; Carroll, W. E.; Teller, R. G.; Koetzle, T. F. *J. Am. Chem. Soc.* **1977**, *99*, 3872−3874.
(19) Cotton, F. A.; Extine, M. W.; Felthouse, T. R.; Kolthammer, B. W. S.; Lay, D. G. *J. Am. Chem. Soc.* **1981**, *103*, 3.

greater detail in the section on bonding considerations and density functional theory calculations.

Species **1** is not particularly reactive, as evidenced by the fact that exposure of solutions of **1** to ethylene or carbon monoxide resulted in no reaction. This lack of reactivity is quite different from that reported for the less coordinatively saturated hydride complex ([NPN]-Ta)$_2$(μ-H)$_4$, which reacts directly with dinitrogen and eliminates 1 equiv of dihydrogen to form a dinitrogen complex.[1] Likewise, complex **1** did not react directly with D_2 gas to form the deuterated analogue ([P_2N_2]Ta)$_2$(μ-D)$_4$; this latter complex was synthesized from the reaction of [P_2N_2]TaMe$_3$ with D_2 gas. A comparison of the IR spectra of the hydride complex **1** and the deuterated species **1**-d_4 did not definitively identify the bridging hydride stretches, as the region in which they were expected was obscured by other peaks associated with the [P_2N_2] ligand. There were no stretches in the IR spectra of **1** or **1**-d_4 in the region normally associated with terminal Ta−H bonds.

Partial Hydrogenation of [P_2N_2]TaMe$_3$. The failure of [P_2N_2]TaMe$_3$ to hydrogenate to form the mononuclear Ta(V) hydride [P_2N_2]TaH$_3$ raises the question as to at what point in the hydrogenation the reduction to Ta(IV) took place. Monitoring the hydrogenation of [P_2N_2]TaMe$_3$ by ^{1}H NMR spectroscopy in a sealed tube under 1 atm of dihydrogen revealed that an intermediate hydrogenation product, **2**, is formed, which is converted entirely to **1** over 3 days. Performing the hydrogenation of [P_2N_2]TaMe$_3$ in a sealed NMR tube under 0.5 atm of dihydrogen resulted in a pale orange solution after 1 week. Unlike the hydrogenation under 1 atm of H_2, the ^{31}P{^{1}H} NMR spectrum indicates that under these conditions very little of **1** is formed, and the solution is mostly a mixture of the starting material and the hydrogenation intermediate **2**.

Unfortunately, attempts to isolate and purify this intermediate have failed. Logical candidates for this presumed Ta(V) species are the partially hydrogenated species [P_2N_2]TaMe$_2$(H) and [P_2N_2]TaMe(H)$_2$, although hydride-bridged dimers of these compounds are also a possibility.[20] The ^{31}P{^{1}H} NMR spectrum displays two phosphorus-31 environments for **2**, coupled to each other with a 125 Hz coupling constant. Prominent in the ^{1}H NMR spectrum of the hydrogenation intermediate is a peak at 5.68 ppm, the same region in which the bridging hydrides in **1** were observed; no coupling to phosphorus-31 could be resolved. Attempts to obtain an accurate integration of this peak proved to be difficult. An inversion−recovery measurement of the T_1 relaxation times for the ^{1}H spectrum indicated that the hydridic proton relaxed much more slowly than the ligand protons. From inversion−recovery experiments, the T_1 value of this hydride signal is estimated to be ∼20 s at room temperature in a 500 MHz spectrometer. The integration of this peak from a ^{1}H NMR spectrum obtained with an increased delay time, compared with the integration of the peaks associated with the ortho protons of the PPh groups and the new tantalum methyl group at δ 0.88, supports an empirical formula of [P_2N_2]-TaMe$_2$(H).

Various aspects of the data, such as the small coupling constant of the hydride resonance to phosphorus[21,22] and the long T_1 value for the hydride resonance, could be construed to imply a dimeric structure,[23] although the correlation between structure and T_1 relaxation times of metal hydrides is fraught with uncertainty.[24,25] Likewise, the two phosphorus environments observed in the ^{31}P{^{1}H} NMR spectrum is consistent with an eight-coordinate dimeric structure rather than the seven-coordinate monomer, which would likely be fluxional and have only one phosphorus environment at room temperature.[5] Unfortunately, no definitive data exist to confirm either a monomeric or a dimeric structure for complex **2**.

This σ-bond metathesis reaction that forms **2** could also be performed using silanes. The reaction of [P_2N_2]-TaMe$_3$ with Bu^{n}SiH$_3$ also produced **1** and intermediate **2**, but not as cleanly as the reactions with dihydrogen. During the reaction of [P_2N_2]TaMe$_3$ with Bu^{n}SiH$_3$, intermediate **2** accumulates in a larger amount relative to the concentration of **1** than in the analogous hydrogenation reaction, consistent with the much slower reaction of the bulkier Bu^{n}SiH$_3$ with intermediate **2** than with dihydrogen.

Synthesis and Structure of {([P^2N_2]Ta)$_2$(μ-H)$_4$}$^+$I$^-$ (3). The reaction of alkyl halides with transition-metal hydrides is a well-known reaction; the formation of a new C−H bond and a metal halide complex has been used as a diagnostic and quantitative test for metal hydride complexes.[26−28] It was anticipated that this reaction could also be used in a synthetic manner to produce a [P_2N_2]Ta^{IV} halide starting material, such as ([P_2N_2]TaI$_2$)$_x$. The reaction of a toluene solution of **1** with excess MeI resulted in the precipitation of an insoluble crystalline paramagnetic green solid, **3**. This solid dissolved in CH_2Cl_2 to give a dichroic solution from which transmitted light appears blue-green and reflected light appears red. In contrast to our expectations, X-ray crystallography identified the compound as {([P_2N_2]Ta)$_2$(μ-H)$_3$}$^+$I$^-$, a cationic hydride, with three hydride ligands bridging the tantalum metal centers. The paramagnetism would be explained if there were no metal−metal bond between the two Ta(IV) centers. The overall reaction would then be the result of the electrophilic abstraction of a hydride ligand by CH_3I, with 1 equiv of CH_4 being produced in the reaction. However, X-ray crystallography is not always a reliable method for determining hydride ligand locations, and as one of the hydrides in this solution to the X-ray data lies on a symmetry element, where errors in electron density often accumulate, the structure could not be accepted without further study. A second possible

(20) Mayer, J. M.; Wolczanski, P. T.; Santarsiero, B. D.; Olson, W. A.; Bercaw, J. E. *Inorg. Chem.* **1983**, *22*, 1149−1155.

(21) Crabtree, R. H. *Acc. Chem. Res.* **1979**, *12*, 331.

(22) Bau, R.; Carroll, W. E.; Hart, D. W.; Teller, R. G.; Koetzle, T. F. *Adv. Chem. Ser.* **1978**, *No. 167*, 73−92.

(23) Bakhmutov, V. I.; Vorontsov, E. V.; Nikonov, G. I.; Lemenovskii, D. A. *Inorg. Chem.* **1998**, *37*, 279−282.

(24) Crabtree, R. H.; Segmuller, B. E.; Uriarte, R. J. *Inorg. Chem.* **1985**, *24*, 1949−1950.

(25) Hlatky, G. G.; Crabtree, R. H. *Coord. Chem. Rev.* **1985**, *65*, 1−48.

(26) Collman, J. P.; Hegedus, L. S.; Norton, J. R.; Finke, R. G. *Principles and Applications of Organotransition Metal Chemistry*; University Science Books: Mill Valley, CA, 1987.

(27) Cotton, F. A.; Wilkinson, G. *Advanced Inorganic Chemistry*, 5th ed.; Wiley-Interscience: New York, 1988; p 1105.

(28) Crabtree, R. H. *The Organometallic Chemistry of the Transition Metals*, 2nd ed.; Wiley-Interscience: New York, 1994; p 62.

product is the result of the one-electron oxidation of **1** to produce $\{([P_2N_2]Ta)_2(\mu\text{-}H)_4\}^+I^-$, a cationic tetrahydride in which one of the electrons in the tantalum−tantalum bond has reduced MeI by one electron, to produce I^- and a methyl radical, which is likely rapidly converted to methane by reaction with the solvent. This compound should be paramagnetic regardless of whether the electron resides in a tantalum−tantalum bonding orbital, because the formal oxidation state of the two metal centers is now intermediate between Ta(IV) and Ta(V).

A variety of approaches were taken to ascertain the nature of **3**. Protonation of a hydride is a common route to cationic hydrides and proceeds via hydride abstraction. Similar to the reaction of CH_3I with **1**, the reaction of **1** with $H^+\{B[3,5\text{-}(CF_3)_2C_6H_3]_3\}$ also produced a paramagnetic green solid; this solid dissolves in THF to give a solution that exhibits the same dichroic behavior observed for **3**. Conversely, the reaction of **3** with the hydride source $K^+\{BEt_3H\}^-$ regenerates the neutral tetrahydride **1**. Although both of these observed reactivities would be expected if **3** is the cationic trihydride $\{([P_2N_2]Ta)_2(\mu\text{-}H)_3\}^+I^-$, they do not exclude the possibility that **3** is the cationic tetrahydride $\{([P_2N_2]Ta)_2(\mu\text{-}H)_4\}^+I^-$. A more definitive study was performed using deuterium-labeled **1**-d_4, $([P_2N_2]Ta)_2(\mu\text{-}D)_4$, prepared from the reaction of $[P_2N_2]TaMe_3$ with D_2. Reaction of **1**-d_4 with CH_3I did not produce CH_3D, as determined by GS-MS; rather, CH_4 was produced. As additional evidence, the reaction of deuterated **3** with $K^+\{BEt_3H\}^-$ did not produce the partially deuterated **1**-d_3, $([P_2N_2]Ta)_2(\mu\text{-}H)(\mu\text{-}D)_3$, but rather the fully deuterated **1**-d_4, $([P_2N_2]Ta)_2(\mu\text{-}D)_4$. The reaction of **1** with CH_3I or $H^+\{B[3,5\text{-}(CF_3)_2C_6H_3]_3\}$ is therefore not a hydride abstraction reaction, and instead, we can assign compound **3** as the cationic tetrahydride $\{([P_2N_2]Ta)_2(\mu\text{-}H)_4\}^+I^-$. The role of $K^+\{BEt_3H\}^-$ in the reaction with **3** is therefore not as a hydride source but simply as a reducing agent. These two reactions are depicted in Scheme 1. Dibenzyl ($PhCH_2CH_2Ph$) was observed as a product in both reactions by ^1H and $^{13}C\{^1H\}$ NMR spectroscopy.

To add further evidence to the nature of compound **3** and to assess the reducing ability of the tantalum−tantalum bond in **1**, cyclic voltammetry was performed on both the neutral and the cationic species. The cyclic voltammograms were performed in CH_2Cl_2 containing $\{NBu^n_4\}^+\{PF_6\}^-$ as the electrolyte and were referenced with respect to $(C_5Me_5)_2Fe$ as an internal standard. Both compounds **1** and **3** exhibit two identical one-electron oxidations; one occurs at −1.18 V and the second at −0.33 V relative to the SCE, providing further proof as to the identity of **3**. The cyclic voltammogram for **1** is shown in Figure 3. Species **3** exhibits additional oxidations at 0.23 and 0.61 V, due to oxidation of the counteranion. All the oxidations observed were reversible. The first oxidation of **1** is expected to produce the cation observed in **3**; the second oxidation indicates that the species $\{([P_2N_2]Ta)_2(\mu\text{-}H)_4\}^{2+}$, which contains two Ta(V) metal centers and no electrons in a Ta−Ta bonding orbital, is also stable. The large separation between the two oxidation potentials is as expected for a case where the single electron is delocalized in a metal−metal bond between the two tantalum atoms,

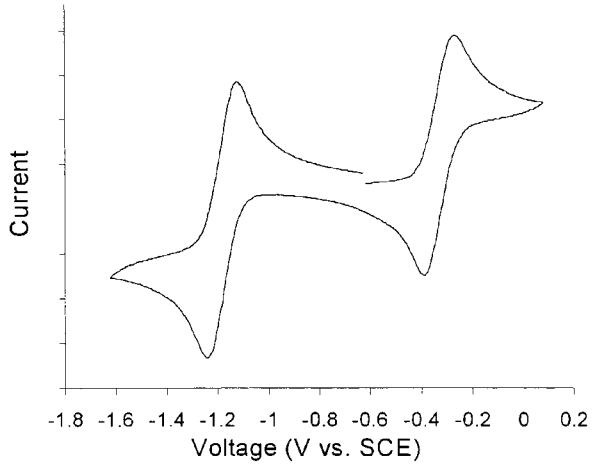

Figure 3. Cyclic voltammogram for $([P_2N_2]Ta)_2(\mu\text{-}H)_4$ (**1**). The cyclic voltammogram of **3** shows identical one-electron oxidation waves. Note that where the scan begins, at −0.6 V, species **1** has already been oxidized to **3** at the electrode.

Scheme 1

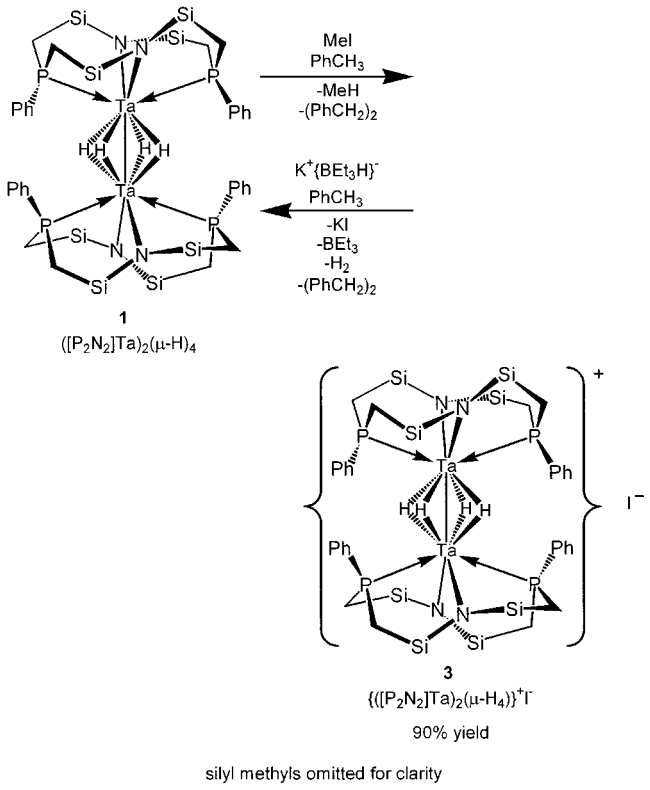

rather than a structure that contains localized Ta(IV) and Ta(V) metal centers.

Compound **3** is moderately air stable; dilute solutions in CH_2Cl_2 only lose color after several hours when exposed to atmospheric oxygen. In fact, upon exposure of CH_2Cl_2 solutions of **1** to air, a distinctive dichroic solution results that is indicative of the cation in complex **3**. Solutions of **3** do not react with simple small molecules such as ethylene or carbon monoxide; this lack of reactivity provides indirect evidence that the dinuclear nature of **3** is maintained in solution.

The solid-state molecular structure of **3** as determined by X-ray crystallography is shown in Figure 4. Crystallographic data are given in Table 1. The molecule has crystallographic C_2 symmetry, with the C_2 axis passing

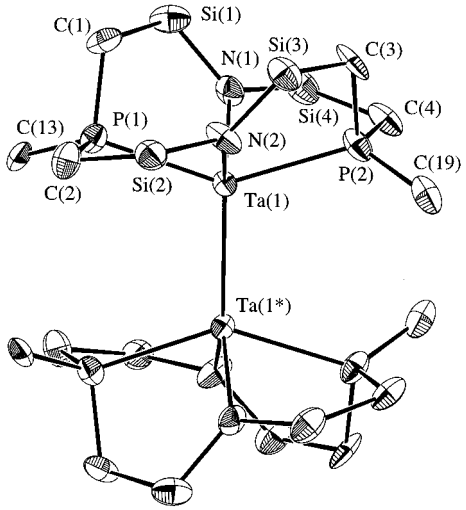

Figure 4. ORTEP diagram of the solid-state molecular structure of the cationic fragment of $\{([P_2N_2]Ta)_2(\mu\text{-}H)_4\}^+I^-$ (**3**), as determined by X-ray crystallography. Silyl methyls have been omitted for clarity, and only the ipso carbons of the phenyl rings attached to phosphorus are shown. The bridging hydrides were not located. Selected bond distances (Å), bond angles (deg), and torsion angles (deg): Ta(1)−Ta(1)*, 2.7721(5); Ta(1)−P(1), 2.602(2); Ta(1)−N(1), 2.145(5); P(1)−Ta(1)−P(2), 143.58(5); Ta(1)*−Ta(1)−P(1), 108.91(4); N(1)−Ta(1)−N(2), 102.4(2); Ta(1)*−Ta(1)−N(1), 127.25(12); P(1)−Ta(1)−Ta(1)*−P(1)*, −2.81(10); N(1)−Ta(1)−Ta(1)*−N(1)*, −8.9(5); Ta(1)−Ta(1)*−N(1)*−Si(1)*, 129.6(4).

through the center of the molecule and parallel to the plane containing the four phosphine ligands. The arrangement of the ancillary $[P_2N_2]$ ligands in the cationic portion of species **3** is remarkably similar to that in **1**. The phosphine ligands on opposing metal centers are eclipsed with a P(1)−Ta(1)−Ta(1)*−P(1)* torsion angle of −2.81(10)°. The P(1)−Ta(1)−P(2) angle of 143.58(5)° and the N(1)−Ta(1)−N(2) angle of 102.4(2)° are also nearly identical with those observed in **1**. The Ta(1)−P(1) distance of 2.602(2) Å is only about 0.01 Å shorter than the Ta−P distances in **1**, whereas the Ta(1)−N(1) distance of 2.145(5) Å is shorter by 0.054 Å than the Ta(1)−N(1) distance in **1**, perhaps due to the increased positive charge on the tantalum centers strengthening the bonds to these anionic ligands, or perhaps from the availability of an extra orbital of correct symmetry to overlap with occupied amide lone-pair orbitals. The twist in the ligand conformation present in **1** is also observed in the solid-state structure of **2**, with an identical Ta(1)−Ta(1)*−N(1)*−Si(1)* torsion angle of 129.6(4)°. The iodide anion has no close contacts with the metal centers. Despite the remarkable similarity between the arrangement, bond angles, and bond lengths in the $[P_2N_2]$Ta fragments of the solid-state structures of **1** and **3**, a significantly longer Ta−Ta distance is observed. The Ta(1)−Ta(1)* distance of 2.7721(5) Å in the tetrahydride cation **3** is 0.156 Å longer than the Ta(1)−Ta(2) distance in the neutral tetrahydride **1**, despite the absence of only a single bonding electron.

The ^{1}H NMR spectrum of species **3** in CD_2Cl_2 contains only broad paramagnetically shifted peaks; though over time CH_2Cl_2 solutions of **3** decompose to yield colorless diamagnetic products. As has been noted, solutions of **3** in CH_2Cl_2 are dichroic; this behavior has been

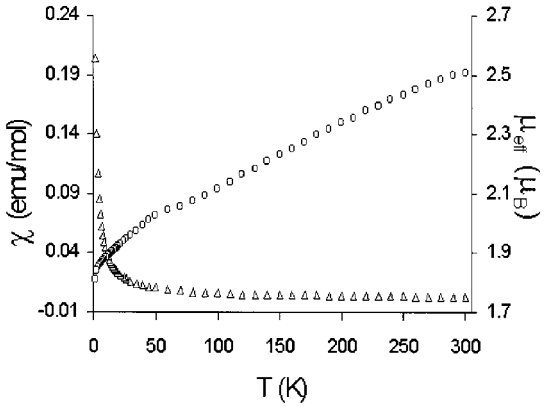

Figure 5. Measured molar magnetic susceptibilities, χ (Δ), and effective magnetic moments, μ_{eff} (○), versus temperature for $\{([P_2N_2]Ta)_2(\mu\text{-}H)_4\}^+I^-$ (**3**).

observed before for other paramagnetic species.[29] The solution and solid-state EPR spectra provide little structural data, as both contain a very broad signal, with no hyperfine or superhyperfine coupling to tantalum, phosphorus, or hydrogen resolved. The solid-state EPR contains a signal at a *g* value of 1.89 with a very large half-height width of 800 G. In contrast, the monomeric Ta(IV) complex $TaH_4(dmpe)_2$ reportedly exhibits hyperfine coupling to ^{181}Ta (99.99%, $I = {}^7/_2$, $a_{Ta} = 106.3$ G) and ^{31}P (100.0%, $I = {}^1/_2$, $a_P = 32.9$ G),[30] and the related dinuclear complex $\{[(PEt_2Ph)_2H_2Re]_2(\mu\text{-}H)_4\}^+$ contains a complex spectrum due to one unpaired electron that resides in a Re−Re bonding orbital and therefore couples to two rhenium nuclei.[31]

Magnetism of $\{([P_2N_2]Ta)_2(\mu\text{-}H)_4\}^+I^-$ (3). Figure 5 shows a plot of χ, the molar magnetic susceptibility corrected for diamagnetic contributions, and μ_{eff}, the effective magnetic moment, for the temperature range of 2−300 K.

Attempts to model the entire data set for **3** with the Curie−Weiss law, using *g*, Θ, and a temperature-independent paramagnetism term (TIP) as parameters, did not provide a good fit. This is possibly due to spin−orbit coupling or perhaps due to the error in the approximation of the diamagnetic correction for species **3**. For the third-row transition elements strong spin−orbit coupling is common, unlike for the first-row transition elements, and is not trivial to model. While there are no strictly degenerate orbitals on the individual tantalum metal centers that would allow for a large contribution from first-order spin−orbit coupling, low-lying orbitals that may be thermally populated could affect the magnetism, leading to a second-order spin−orbit coupling effect. Modeling only the low-temperature data from 2 to 50 K, which should be less affected by thermally dependent second-order spin−orbit coupling, as well as by errors in the diamagnetic correction, the parameters $g = 1.86$, TIP $= 1670 \times 10^{-6}$ emu mol^{-1}, and $\Theta = -0.11$ K were determined. This model is shown in Figure 6. The *g* value is as anticipated from the EPR data, and is consistent with a d^1 metal center where there are no degenerate orbitals present

(29) For example, the ubiquitous ferrocenium ion, $[(C_5H_5)_2Fe]^+$, also exhibits a blue-green/red dichroism.
(30) Allison, J. D.; Walton, R. A. *J. Am. Chem. Soc.* **1984**, *106*, 163.
(31) Allison, J. D.; Walton, R. A. *J. Am. Chem. Soc.* **1984**, *106*, 163−168.

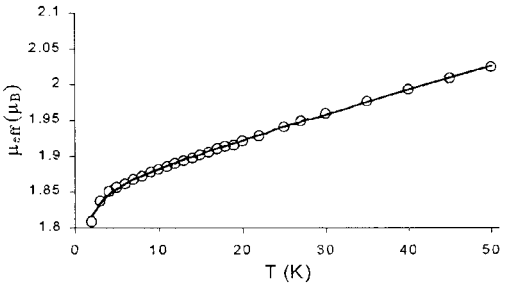

Figure 6. Plot of the effective magnetic moment (μ_{eff}) versus temperature for compound **3** from 2 to 50 K. The circles represent the data points and the bold line a model using the Curie−Weiss law with the parameters $g = 1.86$, TIP $= 1670 \times 10^{-6}$ emu mol^{-1}, and $\Theta = -0.11$ K.

for a large first-order spin−orbit coupling effect. The TIP is responsible for the magnetic moment being much larger than expected for a d^1 complex at room temperature. The negative Θ value indicates that small intermolecular interactions between unpaired electrons on adjacent molecules do in fact occur, although the exact nature of these interactions is unclear.[32,33]

Bonding Considerations and Density Functional Theory Calculations. The bonding of hydride-bridged dinuclear metal complexes has been treated at various levels of theory in the past. A general approach using fragment molecular orbital analysis and supported by extended Hückel theory has been applied to a variety of metals and metal−ligand fragment geometries.[34] A similar analysis supported by a multiple-scattering Xα calculation was performed on $[Cl_2(PH_3)_2Ta]_2(\mu\text{-}H)_4$, a model complex for the species $[Cl_2(PMe_3)_2Ta]_2(\mu\text{-}H)_4$, which is pertinent to the complexes described here.[12] Both methods relied on arbitrary geometries, chosen from relevant crystal structure data, rather than optimized geometries. Both analyses also present a similar approach to describing the bonding in these structures, where the available metal−ligand fragment orbitals are overlapped with the four possible linear combinations of the four bridging hydride ligands. This approach as applied to complex **1** is illustrated in Figure 7.

The orbital analysis for **1** in Figure 7 shows the four linear combinations of the hydride 1s orbitals and the metal-based orbitals that are of the appropriate symmetry for overlap to form three-center σ, π, or δ bonding orbitals. It has been noted previously that the lowest energy fully bonding linear combination of the hydride orbitals is of much lower energy than the metal-based orbitals of appropriate symmetry to form a σ-bonding orbital. The combination of the two metal orbitals of σ-symmetry forms a metal−metal bonding orbital that includes only a small contribution by the bridging hydride ligands. Complex **1** contains 10 electrons that fill these 5 orbitals, and therefore, this complex is diamagnetic and the metal−metal bonding orbital is expected to be the highest in energy. It is worth noting that there is one remaining metal-based d orbital on each metal center that is not considered in either of the two aforementioned bonding descriptions, as it has no significant overlap with the hydride orbitals in either complex.

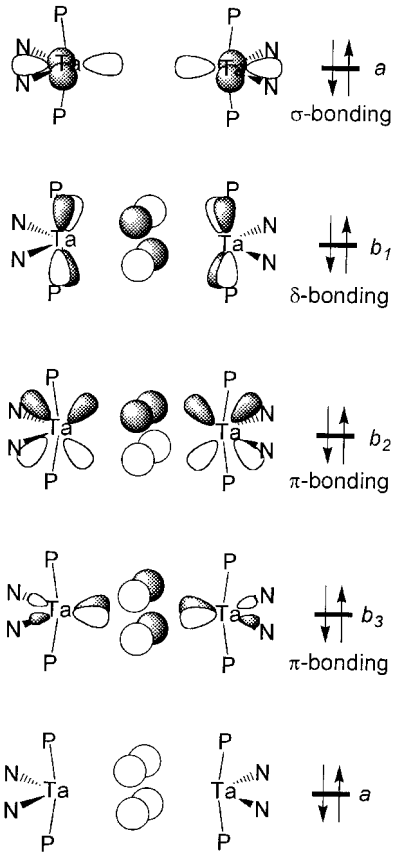

Figure 7. Depiction of the overlap of metal-based orbitals with the bridging hydride ligands to generate delocalized molecular orbitals for complex **1** along with the appropriate symmetry labels for its respective point group (D_2).

The utility of density functional theory (DFT) in modeling compounds of the second- and third-row transition metals that contain metal−metal bonds has recently been demonstrated, even utilizing relatively small basis sets.[35−37] While DFT does not strictly provide molecular orbitals and their respective energies in the same manner as Hartree−Fock calculations, most investigations to date have demonstrated that the resultant Kohn−Sham orbitals are very similar to those predicted by Hartree−Fock theory.[38−42] Therefore, it has been suggested that the Kohn−Sham orbitals of DFT are of equal utility to chemists in the qualitative analysis of reactivity and structure. Even the energies of the Kohn−Sham orbitals appear to be empirically

(32) O'Connor, C. J. *Prog. Inorg. Chem.* **1982**, *29*, 203.
(33) Carlin, R. L. *Magnetochemistry*; Springer-Verlag: Heidelberg, Germany, 1986.
(34) Dedieu, A.; Albright, T. A.; Hoffmann, R. *J. Am. Chem. Soc.* **1979**, *101*, 3141.
(35) Cotton, F. A.; Feng, X. *J. Am. Chem. Soc.* **1997**, *119*, 7514−7520.
(36) Cotton, F. A.; Feng, X. *J. Am. Chem. Soc.* **1998**, *120*, 3387−3397.
(37) Alonso, E.; Casas, J. M.; Cotton, F. A.; Feng, X.; Fornies, J.; Fortuno, C.; Milagros, T. *Inorg. Chem.* **1999**, *38*, 5034−5040.
(38) Stowasser, R.; Hoffmann, R. *J. Am. Chem. Soc.* **1999**, *121*, 3414−3420.
(39) Baerends, E. J.; Gritsenko, O. V.; van Leeuwen, R. In *Chemical Application of Density Functional Theory*; Laird, B. B., Ross, R., Ziegler, T., Eds.; ACS Symposium Series 629; American Chemical Society: Washington, DC, 1996; p 20.
(40) Bickelhaupt, F. M.; Baerends, E. J.; Ravenek, W. *Inorg. Chem.* **1990**, *29*, 350.
(41) DeKoch, R. L.; Baerends, E. J.; Hengelmolen, R. *Organometallics* **1984**, *3*, 289.
(42) Sargent, A. L.; Titus, E. P. *Organometallics* **1998**, *17*, 65.

Table 2. Selected Bond Lengths and Energies for the Ab Initio DFT Geometry Optimizations of 1A

compd	tetrahydride model **1A**
Ta−Ta	2.6444 Å
Ta−H	1.8969, 2.0862 Å
Ta−N	2.0766 Å
Ta−P	2.6680 Å
total energy	−375.1650764 hartree

related to the actual molecular orbital energies.[38] Encouraged by these results, we decided to attempt to model complex **1** using ab initio DFT calculations in order to gain a better understanding of the bonding in this complex. It appeared unusual that the arrangement of the ligands in both **1** and **3** has the phosphine ligands on opposite metal centers eclipsed, rather than staggered by 90° as in the structure of the related complex $[Cl_2(PMe_3)_2Ta]_2(\mu\text{-}H)_4$, and additionally the Ta−Ta bond length in these related species differ by 0.105 Å. Also of interest was the interaction of the amide donors with the metal−metal bonding orbitals. The interactions of π-bonding ligands with multiple bonds between metals are of current interest in generating one-dimensional conducting polymers,[43] and these interactions are of potential importance in the reactivity of other dinuclear $[P_2N_2]$ complexes.[7,8]

Rather than using the $[P_2N_2]$ fragment, complex **1** was modeled using the species $[(H_2N)_2(H_3P)_2Ta]_2(\mu\text{-}H)_4$ (**1A**) to simplify the calculations. Constraints were added to ensure that this complex simulated the geometrically restricted $[P_2N_2]$ macrocycle. The Ta−Ta−P angles were set at 110.0° and the Ta−Ta−N angle at 129.5°, as observed in the solid-state X-ray structure of **1**. In an attempt to simulate the "twist" in the $[P_2N_2]$ ligand noted in **1**, the H−N−Ta−Ta dihedral angle was restrained to 120.0°. Failure to restrict this angle in calculations on **1A** resulted in a H−N−Ta−Ta dihedral near 180°; however, the Si−N−Ta−Ta dihedral angle in the $[P_2N_2]$ macrocycle cannot be that large, due to geometrical restraints in the macrocyclic ring.

The geometry of model complex **1A** was optimized (with the exception of the previously stated constraints) with idealized D_2 symmetry using the Gaussian 98 program[44] and the hybrid functional B3LYP method.[45] The basis functions and effective core potentials (ECP) used were those in the LANL2DZ basis set[46] but with additional d polarization functions added to P atoms with the exponent of the d functions set at 0.37. This level of theory has recently been shown to be adequate for modeling complexes containing metal−metal bonds of various orders, although metal−metal bonds were consistently slightly longer than experimental values.[35]

Selected optimized bond lengths, bond angles, and dihedral angles for the model complex **1A** are shown in Table 2. The general features of the optimized geometry of this model complex are in good agreement with the structure of complex **1**. The arrangement of the ligands on the opposing metal centers as described by the P−Ta−Ta−P dihedral angle 2.37° is similar to that in **1**; the phosphine ligands on opposing metal centers are essentially eclipsed. The calculated Ta−Ta distance of 2.644 Å is only slightly longer than the actual Ta−Ta bond length in complex **1** of 2.6165(5) Å.

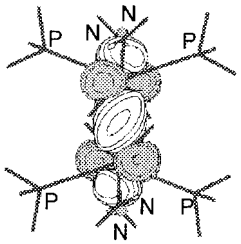

Figure 8. Depiction of the metal−metal σ-bond interaction in the HOMO of tetrahydride **1A**. The PH_3 and NH_2 donors are labeled by P and N, respectively. The frontmost NH_2 ligand on each tantalum center obscures the view of the rear NH_2 ligand.

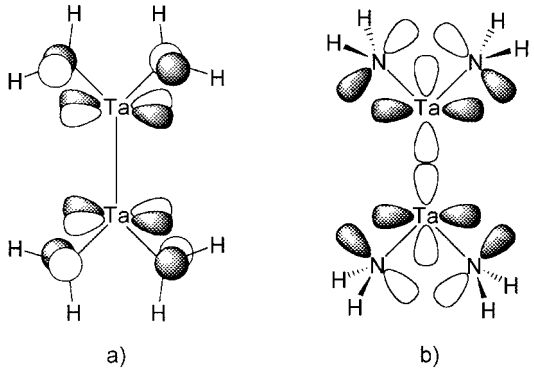

Figure 9. Illustration of the amide lone-pair orbital overlaps for model **1A** when the H−N−Ta−Ta dihedral angle is 180° (a) and when the H−N−Ta−Ta dihedral angle is 90° (b), depicted in the N−Ta−N plane. The PH_3 donors and bridging hydrides are omitted.

The Kohn−Sham orbitals obtained from the geometry optimization for **1A** appear to qualitatively fit the bonding description for **1** shown in Figure 7; however, several other interesting features appear, such as the influence of the amido "lone pairs" (occupied p orbitals on the amido donors) on the bonding in **1A**. The HOMO of **1A** is the Ta−Ta bonding orbital, as anticipated. An isosurface of this orbital is shown in Figure 8 and clearly shows good orbital overlap between the two metal orbitals. There is very little contribution from the bridging hydride 1s orbitals in the HOMO. The ensemble of hydride orbitals of appropriate symmetry lies much lower in energy.

The next lowest energy orbitals for **1A** are different symmetry combinations of the nonbonding electrons on the amido ligands. The interaction of the amido lone pairs with metal-based orbitals was ignored in the model shown in Figure 7; however, these calculations demonstrate that they are not negligible. It was mentioned previously that attempts to optimize the geom-

(43) Chisholm, M. H. *Acc. Chem. Res.* **2000**, *33*, 53.
(44) Frisch, M. J.; Trucks, G. W.; Schlegel, H. B.; Scuseria, G. E.; Robb, M. A.; Cheeseman, J. R.; Zakrzewski, V. G.; Montgomery, J. A.; Stratmann, R. E.; Burant, J. C.; Dapprich, S.; Millam, J. M.; Daniels, A. D.; Kudin, K. N.; Strain, M. C.; Farkas, O.; Tomasi, J.; Petersson, V. A.; Ayala, P. Y.; Cui, Q.; Morokuma, K.; Malick, D. K.; Rabuck, A. D.; Raghavachari, K.; Foresman, J. B.; Cioslowski, J.; Ortiz, J. V.; Stefanov, B. B.; Liu, G.; Liashenko, A.; Piskorz, P.; Komaromi, I.; Gomperts, R.; Martin, R. L.; Fox, D. J.; Keith, T.; Al-Laham, M. A.; Peng, C. Y.; Nanayakkara, A.; Gonzalez, C.; Challacombe, M.; Gill, P. M. W.; Johnson, B. G.; Chen, W.; Wong, M. W.; Andres, J. L.; Head-Gordon, M.; Repogle, E. S.; Pople, J. A. Gaussian 98, Revision A.7; Gaussian, Inc., Pittsburgh, PA, 1998.
(45) Becke, A. D. *J. Chem. Phys.* **1993**, *98*, 5648.
(46) Hay, P. J.; Wadt, W. R. *J. Chem. Phys.* **1985**, *82*, 270.

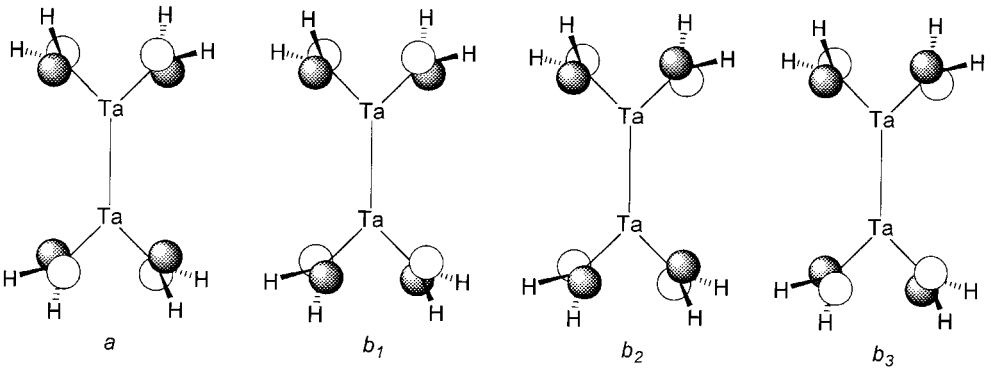

Figure 10. Four possible linear combinations of the nitrogen lone-pair orbitals in **1A**, in D_2 symmetry, depicted in the N−Ta−N plane, along with their symmetry labels. The PH_3 donors and bridging hydrides are not shown.

etry of **1A** with no restriction on the H−N−Ta−Ta dihedral angle resulted in a dihedral angle of 180°. The amide lone pairs in this situation have good overlap with the δ symmetry orbitals (labeled b_1 in Figure 7), as illustrated in Figure 9a). As mentioned, the backbone of the $[P_2N_2]$ macrocycle renders this conformation impossible. If the H−N−Ta−Ta dihedral angle is near 90°, the best overlap now occurs with the metal-based σ-bonding orbitals (the highest energy orbital of a symmetry in Figure 7: this overlap is illustrated in Figure 9b).

In the case of the actual model **1A**, the H−N−Ta−Ta dihedral angle was restricted to 120° in an attempt to simulate the conformational restrictions of the macrocyclic $[P_2N_2]$ ligand. Therefore, overlap with both the metal orbitals in Figure 9 is possible, although each overlap may be poorer than illustrated in Figure 9. There are four possible linear combinations of the amide π-donor orbitals, and these are shown in Figure 10. These have a, b_1, b_2, and b_3 symmetry, respectively.

There are orbitals of each of these symmetries in model complex **1A**, as can be seen from Figure 7; however, the b_2 and b_3 symmetry metal−hydride π-bonding orbitals are too low in energy for a large interaction with the amide lone-pair orbitals. Therefore, in model complex **1A** the two highest energy amide lone-pair orbitals, HOMO-1 and HOMO-2, are of b_2 and b_3 symmetry and do not have a significant contribution from any metal-based orbital. The next lowest energy symmetry combination of the amido lone pair is of a symmetry and has some overlap with the metal−metal orbital of a symmetry similar to the HOMO orbital. This metal orbital has already been used to form the metal−metal bond of the HOMO orbital. There is a slight antibonding contribution from the lone pair orbital to the metal center in the HOMO, so that overall this interaction does not greatly strengthen metal−amide bonding. The first three symmetry combinations of the amido donors are shown in Figure 11.

The fourth symmetry combination of the amido lone pairs is b_1, which is the correct symmetry to overlap with the δ-bonding interaction between metal centers. This metal orbital is also occupied and involved in δ bonding with the hydrides. This overlap results in two occupied orbitals delocalized over the nitrogen donors, the tantalum centers, and the hydrides, as shown in Figure 12.

Along with the σ-bonding and δ-bonding interactions in the $Ta_2(\mu\text{-H})_4$ moiety, there are also two strong

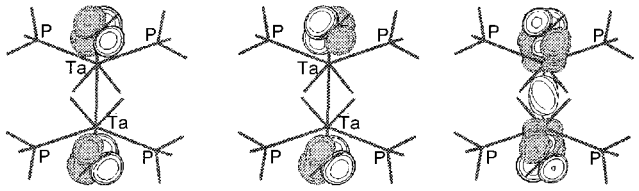

Figure 11. Depictions of the molecular orbitals containing three of the four possible linear combinations of the amido "lone-pair" p orbitals for tetrahydride **1A**. The front NH_2 groups and their π-donor lone-pair orbitals obscure the view of the back NH_2 groups.

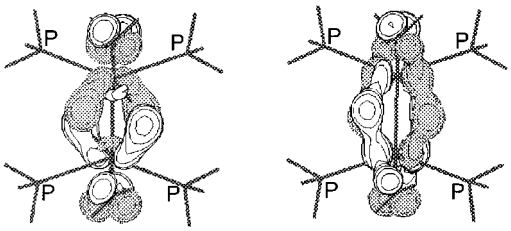

Figure 12. Depiction of the overlap of the fourth symmetry combination of the amido "lone-pair" p orbitals with the metal orbitals involved in δ bonding through the hydride ligands for tetrahydride **1A**.

π-bonding interactions in **1A**, as anticipated. These are shown in Figure 13. These π-bonding interactions are likely responsible for the eclipsed phosphines on the opposite metal centers. In compound **1A** it is not clear that the σ- or δ-bonding interaction should lead to a preference in the arrangement of the ligands on the opposing metal centers (i.e. if the phosphines are eclipsed or staggered by 90°). If the energies of the two π-interactions are largely disparate, as for **1A**, the eclipsed conformation should be favored, as observed here.

An interesting aspect of the $[P_2N_2]$ ligand is that the orientation in which amido lone-pair orbitals are directed is restricted to a very small range. The bonding of the amido lone-pair orbitals appears to destabilize the metal σ-bonding orbital relative to the other remaining metal d orbitals. This destabilization may be responsible for the longer Ta−Ta distance in **1** compared

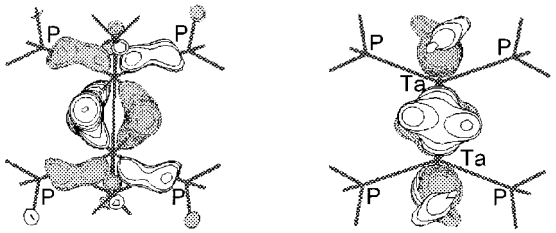

Figure 13. Depiction of the two π interactions between metal centers mediated by the bridging hydride ligands for the tetrahydride model complex **1A**.

to $[Cl_2(PMe_3)_2Ta]_2(\mu\text{-}H)_4$,[12] because in **1** the bridging hydride, amide lone-pair and metal-based electrons must vie for bonding with the same metal orbitals. A further result of this competition of the amide donors with the metal−metal bonding orbital should be an increased reduction potential as compared to that in the absence of these strong π-donors.

Conclusions

The hydrogenation of $[P_2N_2]TaMe_3$ produces the Ta(IV) dimer $([P_2N_2]Ta)(\mu\text{-}H)_4$, which contains a tantalum−tantalum bond. Attempts to react this species with electrophiles such as MeI and $H^+\{B[3,5\text{-}(CF_3)_2C_6H_3]_3\}$ led only to the oxidation of $([P_2N_2]Ta)(\mu\text{-}H)_4$ to produce, in the case of the reaction with MeI, $\{([P_2N_2]Ta)_2(\mu\text{-}H)_4\}^+I^-$. This reaction involves the loss of one electron from the tantalum−tantalum bond. Cyclic voltammetry demonstrates that both electrons in the tantalum−tantalum bond can be removed, to generate $([P_2N_2]Ta)_2(\mu\text{-}H)_4^+$ and $([P_2N_2]Ta)_2(\mu\text{-}H)_4^{2+}$, respectively, and this allows for the quantification of the reducing power of these metal−metal bonding electrons. DFT calculations indicate that the overlap of the amide lone-pair orbitals with the metal−metal bonding orbitals has an influence on the orbital energies, an effect that may have importance in other related systems where electrons stored in metal−metal bonds are used to reduce dinitrogen, such as the closely related system, $([NPN]Ta)_2(\mu\text{-}H)_4$.[1]

Experimental Section

Unless otherwise stated, all manipulations were performed under an atmosphere of dry oxygen-free dinitrogen by means of standard Schlenk or glovebox techniques (Vacuum Atmospheres HE-553-2 glovebox equipped with a MO-40-2H purification system and a −40 °C freezer). Most solvents were dried under argon; however, using a dinitrogen atmosphere does not interfere. Hexanes were predried by refluxing over CaH_2 and then distilled under argon from sodium benzophenone ketyl with tetraglyme added to solubilize the ketyl. Anhydrous diethyl ether was stored over 4 Å molecular sieves and distilled from sodium benzophenone ketyl under argon. Toluene was predried by refluxing over CaH_2 and then distilled from sodium under argon. Nitrogen was dried and deoxygenated by passing the gases through a column containing molecular sieves and MnO. Deuterated benzene and toluene were dried by refluxing with molten potassium metal and molten sodium metal, respectively, in a sealed vessel under partial pressure and then trap-to-trap distilled and freeze−pump−thaw-degassed three times. Unless otherwise stated, ^1H, ^{31}P, $^1H\{^{31}P\}$, $^{13}C\{^1H\}$, ^{13}C, and variable-temperature NMR spectra were recorded on a Bruker AMX-500 instrument operating at 500.1 MHz for ^1H spectra. ^1H NMR spectra were referenced to internal C_6D_5H (7.15 ppm), $CDHCl_2$ (5.32 ppm), and C_7D_7H (2.09 ppm) and $^{31}P\{^1H\}$ NMR spectra to external $P(OMe)_3$ (141.0 ppm with respect to 85% H_3PO_4 at 0.0 ppm). Solution and solid-state EPR spectra were recorded on a Bruker ECS 106. Mr. P. Borda of this department performed the elemental analyses.

Variable-temperature magnetic susceptibility data were collected on a Quantum Design (MPMS) SQUID magnetometer. Magnetic susceptibilities were corrected for the background signal of the sample holder and for diamagnetic susceptibilities of all atoms (-870×10^{-6} emu·mol^{-1}). Measurements were made from 2 to 300 K and at a field strength of 10000 G on a microcrystalline sample that had been ground into a fine powder.

The compound $[P_2N_2]TaMe_3$ was prepared as previously described.[5] Methyl iodide was purchased from Aldrich, degassed via three freeze−pump−thaw cycles and stored over copper wire.

Synthesis of $([P_2N_2]Ta)_2(\mu\text{-}H)_4$ (1). A yellow solution of $[P_2N_2]TaMe_3$ (1.0 g, 1.3 mmol) in 200 mL of hexanes was transferred to a 400 mL thick-walled glass reaction vessel equipped with a Teflon valve and a stir bar. The solution was degassed by two freeze−pump−thaw cycles. With the solution frozen in a liquid N_2 bath, 1 atm of hydrogen gas was added and allowed to cool for 20 min. The Teflon valve was then sealed, and the solution was warmed to room temperature, to produce a hydrogen pressure of 4 atm. Once at room temperature the solution was stirred rapidly, and within 30 min the solution turned dark red and a microcrystalline precipitate formed. After 2 days the hydrogen gas was removed and the brick red precipitate was collected by filtration, rinsed with 10 mL of hexanes, and dried under vacuum, giving $([P_2N_2]Ta)_2(\mu\text{-}H)_4$ in 80% yield. The dark brown hexane rinse did not appear to contain any NMR-active species. Species **1** has only trace solubility in hexanes and is moderately soluble in aromatic solvents. Single crystals suitable for X-ray analysis were obtained by performing the reaction without stirring. ^1H NMR (500 MHz, C_7H_8, 25 °C): δ 0.230, 0.228, 0.46, and 1.17 (s, 48H total, SiCH_3), 0.66 and 0.99 (ABX, $^2J_{HH} = 13.5$ Hz, 8H total, CH_2 ring), 1.04 and 1.43 (ABX, $^2J_{HH} = 13.1$ Hz, 8H total, CH_2 ring), 5.86 (q, $^2J_{PH} = 9.9$ Hz, 4H, *μ-H*), 7.13 (m, 12H, *m-/p-H*), 7.42 (m, 8H, *o-H*). $^{31}P\{^1H\}$ NMR (C_7H_8, 25 °C): δ 10.75. UV/vis (toluene; λ (nm), ϵ): 455, 6200; 348, 8600; 313, 18 000. Anal. Calcd for $C_{24}H_{44}N_2P_2Si_4Ta$: C, 40.27; H, 6.19; N, 3.91. Found: C, 40.37; H, 6.34; N, 3.85.

$([P_2N_2]Ta)_2(\mu\text{-}D)_4$ (1-*d*$_4$). The deuterated analogue of **1** was prepared in an identical manner using D_2 gas in lieu of H_2 gas.

$[P_2N_2]TaMe_2(H)$ (2). A yellow solution of $[P_2N_2]TaMe_3$ (20 mg) in 1 mL of C_6D_6 was sealed in a NMR tube under 0.5 atm of hydrogen gas using a vacuum manifold equipped with a mercury manometer and stirred in the absence of light for 1 week. The resulting solution was identified by ^1H and $^{31}P\{^1H\}$ NMR as having the empirical formula $[P_2N_2]TaMe_2(H)$. ^1H NMR (500 MHz, C_6H_6, 25 °C): δ 0.06, 0.22, 0.39, and 0.46 (s, 24H total, SiCH_3), 0.88 (dd, $^2J_{HP} = 7$ Hz, $^2J_{HP} = 7$ Hz, 6H, TaCH_3), 0.93, 1.34, 1.39 and 1.90 (dd, 8H total, SiCH_2P), 5.68 (s, $w_{1/2} = 4.0$ Hz, 1H, $Ta_2(\mu\text{-}H)$), 7.11 (overlapping multiplets, *m-/p-H*), 7.47 (m, 2H, PPh *o-H*), 7.79 (m, 2H, PPh *o-H*). ^{31}P NMR (C_6H_6, 25 °C): δ 17.2 (d, $^2J_{PP} = 125$ Hz), 24.4 (d, $^2J_{PP} = 125$ Hz).

Synthesis of $\{([P_2N_2]Ta)_2(\mu\text{-}H)_4\}^+I^-$ (3). A stirred solution of $[P_2N_2]Ta(\mu\text{-}H)_4$ (0.429 g, 0.300 mmol) in 60 mL of toluene was degassed, and then a large excess of MeI was added by vacuum transfer. Over 3 h the dark solution went colorless and a green microcrystalline solid precipitated. The toluene and excess MeI were removed under vacuum. The solid was collected on a glass filter and rinsed with 20 mL of toluene and then 20 mL of hexanes. The remaining green solid was dried under vacuum, yielding $\{([P_2N_2]Ta)_2(\mu\text{-}H)_4\}^+I^-$ (0.420 g,

90%). This green solid is insoluble in aromatic solvents and tetrahydofuran but soluble in methylene chloride, though solutions decompose over the course of 1 week to give a colorless solution. Methylene chloride solutions of **3** are dichroic; reflected light appears burgundy and transmitted light is blue-green. Single crystals suitable for X-ray analysis were obtained by performing the synthesis in an identical manner, but without stirring. Anal. Calcd for $C_{48}H_{88}N_4P_4Si_8Ta_2$: C, 37.01; H, 5.63; N, 3.60. Found: C, 37.25; H, 5.45; N, 3.47. UV/vis (toluene; λ (nm), ϵ): 576, 2900; 450, sh; 346, 16 000; 298, 15 000. EPR (solid, 295 K): $g = 1.88$, $W_{1/2} = 800$ G. EPR (solution, 295 K): $g = 1.89$, broad.

The colorless toluene-soluble reaction products were evaporated to dryness and identified by ^{1}H and ^{13}C{^{1}H} NMR as dibenzyl ($PhCH_2CH_2Ph$). ^{1}H NMR (C_6D_6, 400 MHz, 298 K): δ 2.73 (s, 4H, $PhCH_2CH_2Ph$), 6.98 (m, 4H, *o-H*), 7.05 (m, 2H *p-H*), 7.13 (m, 4H, *m-H*). ^{13}C{^{1}H} NMR (C_6D_6, 298 K): δ 38.1 (s, $PhCH_2CH_2Ph$), 126.2 (s, *p-C*), 128.5 (s, *m-C*), 128.8 (s, *o-C*), 142.0 (s, *ipso-C*).

X-ray Crystallographic Analyses of 1 and 3. Crystallographic data for **1** and **3** appear in Table 1. For **1** the final unit-cell parameters were obtained by least-squares methods on the setting angles for 25 reflections with $2\theta = 20.1-25.4°$. The intensities of 3 standard reflections were measured every 200 reflections. Throughout the data collections the standards decreased by 1.19%. A linear correction factor was applied to the data to account for this phenomenon. The data were processed and corrected for Lorentz and polarization effects and absorption.[47] The structure of **1** was solved by heavy-atom Patterson methods and expanded using Fourier techniques. The non-hydrogen atoms were refined anisotropically. The metal hydride atoms were refined isotropically, with distance constraints for H(3) and H(4) and a fixed thermal parameter for H(3). The remaining hydrogen atoms were fixed in calculated positions with C−H = 0.98 Å.

For **3** the final unit-cell parameters were obtained by least-squares methods on the setting angles for 33 122 reflections with $2\theta = 4.0-60.1°$ for **3**. The data were processed and corrected for Lorentz and polarization effects. The structure of **3** was solved by direct methods and expanded using Fourier techniques. All the non-hydrogen atoms were refined anisotropically. Metal hydrides were placed in difference map positions but were not refined, and the remaining hydrogen atoms were fixed in calculated positions with C−H = 0.98 Å. The absolute configuration of **3** was determined by Flack parameter refinement (0.014(5)).

(47) teXsan: Crystal Structure Analysis Package; Molecular Structure Corp., The Woodlands, TX, 1995.

Neutral atom scattering factors for the non-hydrogen atoms were taken from refs 48 and 49. Atomic coordinates, anisotropic thermal parameters, complete bond lengths and bond angles, torsion angles, intermolecular contacts, and least-squares planes are included as Supporting Information.

Calculations. The ab initio DFT calculations on the model compound $[(H_2N)_2(H_3P)_2Ta]_2(\mu\text{-}H)_4$ were performed with the hybrid functional B3LYP method[45] using the Gaussian 98 package.[44] The basis functions and effective core potentials (ECP) used were those in the LANL2DZ basis set developed by Hay and Wadt[46] and provided with the Gaussian 98 program, but with an additional d polarization functions added to P atoms. The exponent of the d function was 0.37. This level of theory has recently been shown to be adequate for modeling complexes containing metal−metal bonds of various orders.[35] Model complex **1A** was optimized with D_2 symmetry with the Ta−Ta−P and Ta−Ta−N angles frozen at 110 and 129.5°, respectively, and the H−N−Ta−Ta dihedral angle frozen at 120°. Orbital depictions were created using the MOLDEN program.[50]

Acknowledgment. We gratefully acknowledge both the NSERC of Canada and the Petroleum Research Fund, administered by the American Chemical Society, for funding in the form of research grants. Financial support was also provided by the NSERC of Canada in the form of a postgraduate scholarship for S.A.J., as well as the University of British Columbia in the form of a University Graduate Fellowship. We thank Victor Sanchez for assistance with the use of the SQUID magnetometer as well as Dr. R. C. Thompson for informative discussions on the subject of magnetism.

Supporting Information Available: Text giving full experimental details, tables of X-ray parameters, fractional coordinates and thermal parameters, bond lengths, bond angles, and torsion angles, and ORTEP diagrams for compounds **1** and **3**, variable-temperature magnetic susceptibility data for compound **3**, and full density functional theory results for **1A**. This material is available free of charge via the Internet at http://pubs.acs.org.

OM000359W

(48) *International Tables for X-ray Crystallography*; Kynoch Press: Birmingham, U.K. (present distributor Kluwer Academic: Boston, MA), 1974; Vol. IV.

(49) *International Tables for Crystallography*; Kluwer Academic: Boston, MA, 1992; Vol. C.

(50) Schaftenaar, G. Molden, 3.5 ed.; CAOS/CAMM Center, University of Nijmegen, Nijmegen, The Netherlands, 1991.